

Monte Carlo analysis of MEGA microlensing events towards M31

G. Ingresso¹, S. Calchi Novati², F. De Paolis¹, Ph. Jetzer², A.A. Nucita¹, F. Strafella¹

¹ Dipartimento di Fisica, Università di Lecce and INFN, Sezione di Lecce, CP 193, I-73100 Lecce, Italy

² Institute for Theoretical Physics, University of Zürich, Winterthurerstrasse 190, CH-8057 Zürich, Switzerland

Received / Accepted

Abstract. We perform an analytical study and a Monte Carlo (MC) analysis of the main features for microlensing events in pixel lensing observations towards M31. Our main aim is to investigate the lens nature and location of the 14 candidate events found by the MEGA collaboration. Assuming a reference model for the mass distribution in M31 and the standard model for our galaxy, we estimate the MACHO-to-self lensing probability and the event time duration towards M31. Reproducing the MEGA observing conditions, as a result we get the MC event number density distribution as a function of the event full-width half-maximum duration $t_{1/2}$ and the magnitude at maximum R_{\max} . For a MACHO mass of $0.5 M_{\odot}$ we find typical values of $t_{1/2} \simeq 20$ day and $R_{\max} \simeq 22$, for both MACHO-lensing and self-lensing events occurring beyond about 10 arcminutes from the M31 center. A comparison of the observed features ($t_{1/2}$ and R_{\max}) with our MC results shows that for a MACHO mass $> 0.1 M_{\odot}$ the four innermost MEGA events are most likely self-lensing events, whereas the six outermost events must be genuine MACHO-lensing events.

Key words. Gravitational Lensing; Galaxy: halo; Galaxies: individuals: M31

1. Introduction

Gravitational microlensing has become since about a decade a robust tool for analyzing the galactic structure and for gaining information about the dark mass component in our galaxy (Alcock et al., 1993; Aubourg et al., 1993). Several hundreds of microlensing events have been detected so far towards the galactic bulge, the spiral arms, and the Magellanic Clouds (Alcock et al., 2000; Jetzer et al., 2004).

Recently, pixel lensing observations towards M31 and even M87 have been undertaken and some microlensing events have been found. The MEGA collaboration (de Jong et al., 2004) has reported the detection of 14 candidate events towards M31 by using Isaac Newton Telescope (INT) data. Two of these events have been previously reported by the POINT-AGAPE collaboration (Paulin-Henriksson et al., 2003), which recently has presented a high-threshold analysis of the full 3 years data set (Calchi Novati et al., 2005). This analysis shows that the observed signal is much larger than expect from self-lensing alone and that some fraction of the halo mass must be in form of MACHOs. Other collaborations have also reported preliminary results for pixel lensing towards M31 (Calchi Novati et al., 2002, 2003; Uglesich et al., 2004; Riffeser et al., 2003; Joshi et al., 2004).

In this paper we consider in particular the MEGA results which provide the largest sample of microlensing can-

didates. A map of the MEGA events is reported by de Jong et al. (2004). A preliminary analysis by the MEGA collaboration indicates that the events located in the outer part of M31 are consistent with being due to halo lens objects, whereas the innermost ones are most likely due to self-lensing. The aim of this paper is to perform a more complete analysis by using a Monte Carlo (MC) program with the purpose of using all available information by the MEGA collaboration, which are summarized in Tab. 1, to characterize the nature of the lenses.

The paper is organized as follows: in Section 2 we present the calculation of the microlensing rate towards M31 and we remind the pixel lensing basics. In Section 3 we give some details on the adopted M31 and Milky Way (MW) mass distribution models as well as the stellar and mass functions. The analytic and MC results and a comparison between the two are given in Sections 4-6 and conclusions are presented in Section 7.

2. Microlensing rate

The differential number of expected microlensing events is (De Rújula et al., 1991; Griest, 1991)

$$dN_{\text{ev}} = N_* t_{\text{obs}} d\Gamma, \quad (1)$$

where N_* is the total number of monitored stars during the observation time t_{obs} . The differential rate $d\Gamma$ at which

Table 1. For the 14 MEGA events we give the position, the full-width half-maximum duration $t_{1/2}$ and the magnitude at maximum R_{max} . The coordinate system we adopt has origin in the M31 center and the X axis is oriented along the M31 disk major axis (see also Fig. 1).

MEGA	X arcmin	Y arcmin	$t_{1/2}^{obs}$ day	R_{max}^{obs} magn
1	-4.367	-2.814	4.20 ± 4.30	22.2 ± 1.1
2	-4.478	-3.065	4.60 ± 0.60	21.6 ± 0.3
3	-7.379	-1.659	2.60 ± 2.20	21.8 ± 1.2
4	-10.219	3.420	29.10 ± 1.00	22.8 ± 0.2
5	-19.989	-13.955	9.40 ± 4.10	22.9 ± 0.8
6	-21.564	-13.169	22.90 ± 0.70	22.6 ± 0.2
7	-21.163	-6.230	21.60 ± 0.70	19.3 ± 0.2
8	-21.650	7.670	27.40 ± 0.90	22.7 ± 0.2
9	-33.834	-2.251	3.80 ± 1.60	21.8 ± 0.8
10	-3.933	-13.846	46.80 ± 4.40	22.2 ± 0.3
11	19.192	-11.833	2.00 ± 0.30	20.5 ± 0.2
12	29.781	-5.033	131.00 ± 9.40	23.2 ± 0.3
13	22.072	-22.022	22.80 ± 3.80	23.3 ± 0.3
14	19.348	-29.560	28.10 ± 1.40	22.5 ± 0.2

a single star is microlensed by a compact object is given by

$$d\Gamma = \frac{n_l(\mathbf{x}, \mu) d\mu f(\mathbf{v}_{1\perp}) d^2\mathbf{v}_{1\perp} d^3x}{dt}, \quad (2)$$

where the numerator on the right hand side is the number of lenses with transverse velocity in $d^2\mathbf{v}_{1\perp} = v_{1\perp} dv_{1\perp} d\beta$ around $\mathbf{v}_{1\perp}$, located in a volume element $d^3x = dx dy dz$ centered at the position \mathbf{x} of the microlensing tube. Here $\mathbf{v}_{1\perp}$ is the component (in the rest frame of the Galaxy) of the lens velocity orthogonal to the line of sight to the source star, $n_l(\mathbf{x}, \mu)$ the lens number density (per unit of volume and mass) and $f(\mathbf{v}_{1\perp})$ the lens transverse velocity distribution. μ is the lens mass in solar units.

In evaluating $d\Gamma$ we must take into account that the source stars are not at rest but have a transverse velocity $\mathbf{v}_{s\perp}$ as well, which can be splitted into a random component and a component which describes the ordered rotation (if present) of the galactic component considered, namely $\mathbf{v}_{s\perp} = \mathbf{v}_{s\perp,ran} + \mathbf{v}_{s\perp,rot}$. Using a Maxwellian distribution with 2-dimensional velocity dispersion σ_s to describe the random velocity component, we get for the transverse velocity distribution $g(\mathbf{v}_{s\perp})$

$$g(\mathbf{v}_{s\perp}) v_{s\perp} dv_{s\perp} d\varphi = \frac{1}{\pi\sigma_s^2} e^{-\frac{(\mathbf{v}_{s\perp} - \mathbf{v}_{s\perp,rot})^2}{\sigma_s^2}} v_{s\perp} dv_{s\perp} d\varphi, \quad (3)$$

where φ is the angle between $\mathbf{v}_{s\perp}$ and $\mathbf{v}_{s\perp,rot}$.

We take also into account the transverse rotation velocity of the observer, $\mathbf{v}_{\odot\perp,rot}$ (here we consider the observer co-moving with the Sun) by considering that the microlensing tube is moving with a transverse velocity

$$\mathbf{v}_{t\perp} = \left(1 - \frac{D_{ol}}{D_{os}}\right) \mathbf{v}_{\odot\perp,rot} + \frac{D_{ol}}{D_{os}} \mathbf{v}_{s\perp}, \quad (4)$$

where D_{os} and D_{ol} are the source and lens distances from the observer, respectively.

As for the source stars we split the lens transverse velocity into a random component and an ordered rotation component. Moreover, by taking into account that the microlensing tube moves with velocity $\mathbf{v}_{t\perp}$, it follows that $\mathbf{v}_{1\perp} = \mathbf{v}_{1\perp,ran} + \mathbf{v}_{1\perp,rot} - \mathbf{v}_{t\perp}$. Accordingly, assuming for $\mathbf{v}_{1\perp,ran}$ a Maxwellian distribution with 2-dimensional velocity dispersion σ_l , we obtain using also the definition for $g(\mathbf{v}_{s\perp})$ given in eq.(3)

$$f(\mathbf{v}_{1\perp}) v_{1\perp} dv_{1\perp} d\beta = \frac{1}{(\pi\sigma_s\sigma_l)^2} \int_0^{2\pi} d\varphi \times \int_0^\infty e^{-\frac{(\mathbf{v}_{s\perp} - \mathbf{v}_{s\perp,rot})^2}{\sigma_s^2}} v_{s\perp} dv_{s\perp} e^{-\frac{(\mathbf{v}_{1\perp} - \mathbf{w}_\perp)^2}{\sigma_l^2}} v_{1\perp} dv_{1\perp} d\beta, \quad (5)$$

where $\mathbf{w}_\perp = \mathbf{v}_{1\perp,rot} - \mathbf{v}_{t\perp}$ and β is the angle between $\mathbf{v}_{1\perp}$ and \mathbf{w}_\perp .

We can then write the volume element, d^3x , as

$$d^3x = (\mathbf{v}_{1\perp} \cdot \hat{n}) dt dS = v_{1\perp} \cos\theta dt dl dD_{ol} = v_{1\perp} \cos\theta dt R_E du_{th} d\alpha dD_{ol}, \quad (6)$$

where θ is the angle between $\mathbf{v}_{1\perp}$ and the normal, \hat{n} , to the lateral superficial element, $dS = dl dD_{ol}$, of the microlensing tube, with $dl = R_E du_{th} d\alpha$ being the cylindrical segment of the tube (u_{th} is the threshold value for the impact parameter). Note that, if α is taken to be the angle between \hat{n} and \mathbf{w}_\perp , it follows that $\theta = \alpha + \beta$, so that for a constant value of β , $d\alpha = d\theta$. Therefore, the microlensing differential event rate becomes

$$d\Gamma = n_l(\mathbf{x}, \mu) d\mu f(\mathbf{v}_{1\perp}) v_{1\perp}^2 dv_{1\perp} d\beta \cos\theta R_E du_{th} d\alpha dD_{ol}. \quad (7)$$

We assume, as usual, that the mass distribution of the lenses is independent of their position in M31 or in the Galaxy (*factorization hypothesis*). So, the lens number density $n_l(\mathbf{x}, \mu)$ can be written as (Jetzer et al., 2002)

$$n_l(\mathbf{x}, \mu) = \frac{\rho_l(\mathbf{x})}{\rho_0} \psi_0(\mu), \quad (8)$$

where ρ_0 is the local mass density in the Galaxy or the central density in M31, $\psi_0(\mu)$ the corresponding lens number density per unit of mass and the normalization is

$$\int_{\mu_{min}}^{\mu_{up}} \psi_0(\mu) \mu d\mu = \frac{\rho_0}{M_\odot}. \quad (9)$$

Here μ_{min} and μ_{up} are the lower and the upper limits for the lens masses (see Subsect. 3.3). Accordingly, the microlensing event rate is given by:

$$\Gamma(D_{os}) = \sqrt{\frac{4GM_\odot}{c^2}} \int_{\mu_{min}}^{\mu_{up}} d\mu \mu^{1/2} \psi_0(\mu) \int_0^{u_\tau} du_{th} \times \int_0^{D_{os}} dD_{ol} \sqrt{\frac{D_{ol}(D_{os} - D_{ol})}{D_{os}}} \frac{\rho_l(D_{ol})}{\rho_0} \times \int_0^{2\pi} d\beta \int_0^\infty dv_{1\perp} f(\mathbf{v}_{1\perp}) v_{1\perp}^2 \int_{-\pi/2}^{+\pi/2} \cos\theta d\theta, \quad (10)$$

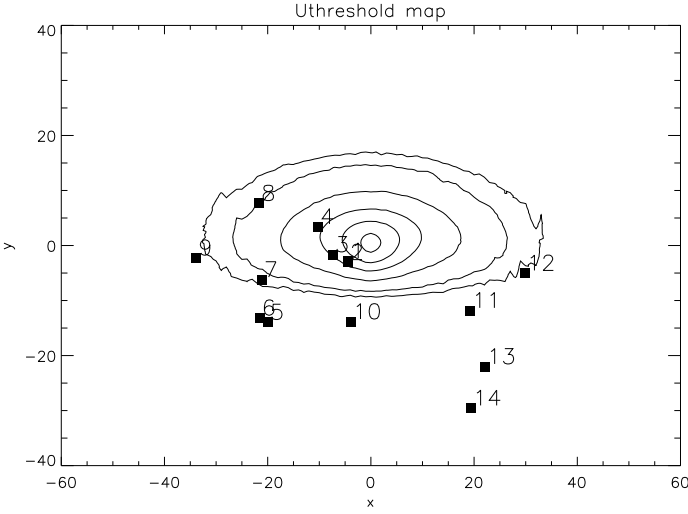


Fig. 1. The $\langle u_T(x, y) \rangle_{\phi_{RG}}$ contour plot towards the M31 galaxy is shown with the position in the sky plane of the 14 MEGA candidate microlensing events. From the inner to the outer part of the figure $\langle u_T(x, y) \rangle_{\phi_{RG}}$ increases with lines referring to the values 0.02, 0.04, 0.06, 0.08 and 0.10, respectively. Outside the 0.10 contour line $\langle u_T(x, y) \rangle_{\phi_{RG}}$ is almost constant. Note that the positions of the events 1 and 2 are almost on top of each other. The same is true as well for all other figures.

where the integration on θ is performed between $-\pi/2$ and $+\pi/2$, since only lenses entering the microlensing tube are considered. After integrations on θ and β we finally get

$$\Gamma(D_{os}) = 2\sigma_1 u_T \sqrt{\frac{4GM_{\odot}}{c^2}} \int_{\mu_{min}}^{\mu_{up}} d\mu \mu^{1/2} \psi_0(\mu) \times \int_0^{D_{os}} dD_{ol} \sqrt{\frac{D_{ol}(D_{os} - D_{ol})}{D_{os}}} \frac{\rho_l(D_{ol})}{\rho_0} \int_0^{\infty} P(z) dz, \quad (11)$$

where $z = v_{1\perp}/\sigma_1$ and the function $P(z)$ is given by

$$P(z) = \frac{2e^{-a^2}}{\pi} \int_0^{2\pi} d\varphi \int_0^{\infty} y e^{-(y^2 - 2ay \cos \varphi + \eta^2)} dy \times z^2 e^{-z^2} I_0(2\eta z). \quad (12)$$

Here $a(D_{os}) = v_{s\perp, rot}/\sigma_s$, $y = v_{s\perp}/\sigma_s$, $\eta(D_{os}, y, \varphi) = w_{\perp}/\sigma_1$ and $I_0(2\eta z)$ is the zero-order modified Bessel function of the argument $2\eta z$.

Note that $\chi(z) = z^{-1}P(z)$ is the dimensionless form of eq. (5) and that it is properly normalized as it can be easily verified by using twice the relation $\int_0^{\infty} dt \exp(-t^2) t I_0(2qt) = \exp(q^2)/2$.

To take into account the source distribution in the M31 bulge and disk, eq. (11) has to be integrated not only over the distance of the lenses but also over the distance of the sources. Accordingly, the microlensing rate becomes

$$\Gamma(x, y) = \frac{\int_0^{\infty} \rho_s(D_{os}) \Gamma(D_{os}) dD_{os}}{\int_0^{\infty} \rho_s(D_{os}) dD_{os}}, \quad (13)$$

where x and y are coordinates in the plane orthogonal to line of sight, ρ_s is the source mass density (which is the sum of the sources in the M31 bulge and disk).

Moreover, we compute the average Einstein time (which depends on the line of sight position given by the coordinates x and y) as

$$\langle t_E \rangle = \frac{\int_0^{\Gamma} t_E d\Gamma}{\Gamma}. \quad (14)$$

2.1. Pixel lensing basics

Pixel lensing technique is based on the observation of the flux variations of every element (pixel) of an image (Ansari et al., 1997). Looking towards M31 a large number of stars contribute at the same time to the flux received by each pixel so that only highly magnified events can be detected.

To be detectable a microlensing event must give rise to a substantial flux variation with respect to the background $N_{bl} = N_{gal} + N_{sky}$, which is the sum of the M31 surface brightness and the sky contribution. The excess photon count per pixel due to an ongoing microlensing event is

$$\Delta N_{pix} = N_{bl}[A_{pix} - 1] = f_{see} N_s [A(t) - 1] \quad (15)$$

where N_s is the source photon count in the absence of lensing, $A(t)$ is the source magnification factor due to lensing (see e.g. Griest 1991) and f_{see} the fraction of the seeing disk contained in a pixel. Therefore, the expected number of photons in a pixel will be $N_{pix} = N_{bl} + \Delta N_{pix}$.

Of course, a pixel lensing event is detectable if the excess pixel photon count is greater than the threshold pixel noise σ_T . Accordingly, by requiring the signal to be at least $3\sigma_T$ level above the baseline count, one obtains a threshold value for the amplification (Kerins et al., 2001)

$$A_T = 1 + \frac{3\sigma_T}{f_{see} N_s}, \quad (16)$$

which corresponds to a threshold value u_T for the impact parameter, via the well known relation between the lens impact parameter and the amplification factor.

One can estimate σ_T as the maximum between the statistical error $\propto \sqrt{N_{bl}}$ and $\simeq 3 \times 10^{-3} N_{bl}$ that is determined by the pixel flux stability. Accordingly, u_T depends on both the line of sight to M31 and the source magnitude M .

Hence, by averaging on the source luminosity function $\phi(M)$, we can evaluate the average threshold impact parameter for any direction towards the M31 galaxy, so that we get

$$\langle u_T(x, y) \rangle_{\phi} = \frac{\int u_T(x, y; M) \phi(M) dM}{\int \phi(M) dM}, \quad (17)$$

where the coordinates x and y span the sky plane towards M31.

By using the threshold impact parameter defined in eq. (17), one obtains the pixel lensing rate as follows (Kerins et al., 2001, 2003; De Paolis et al., 2005)

$$\Gamma_p(x, y) = \langle u_T(x, y) \rangle_{\phi} \Gamma(x, y). \quad (18)$$

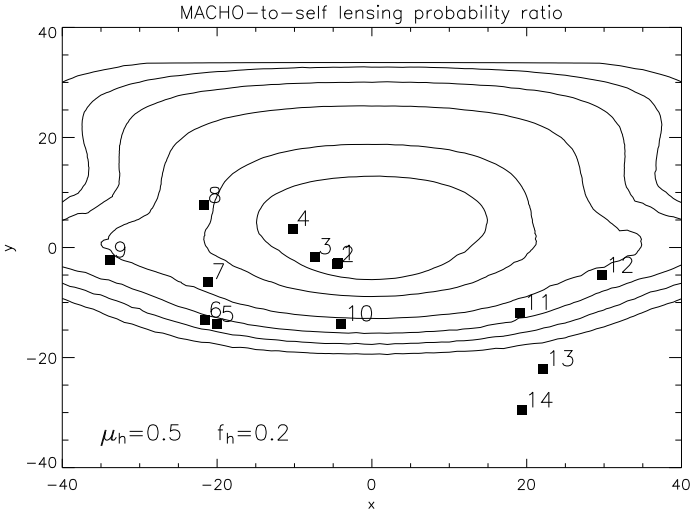


Fig. 2. MACHO-to-self lensing probability ratio $(P_h/P_s)_{An}$ map projected onto the sky plane. Here and in the following figures we assume a fraction $f_h = 20\%$ of dark matter and a MACHO mass $\mu_h = 0.5$, both in M31 and MW halos. From the inner to the outer part $(P_h/P_s)_{An}$ increases with lines referring to the values 0.5, 1, 2, 3, 4 and 5, respectively.

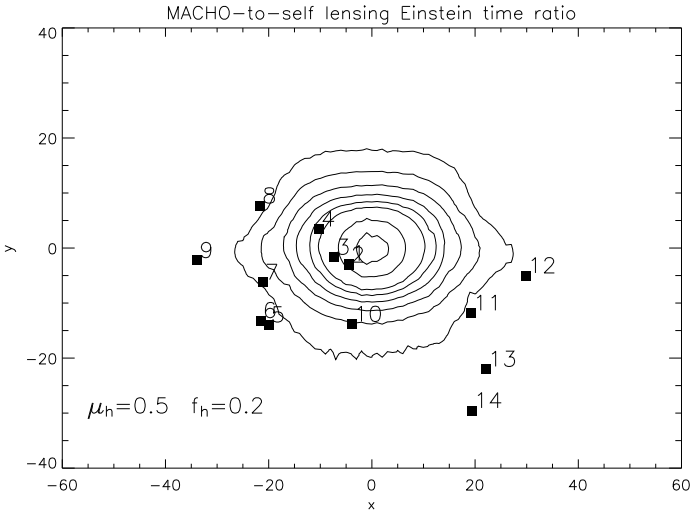


Fig. 3. The MACHO-to-self lensing Einstein time ratio $\langle t_{Eh} \rangle / \langle t_{Es} \rangle$ map is given for $\mu_h = 0.5$. Going from the inner to the outer part the ratio decreases with lines corresponding to values in between 2 to 1.25 with a step of 0.25.

3. Modeling

3.1. M31 and Galaxy mass distribution models

The M31 disk, bulge and halo mass distributions are described adopting the reference model discussed in Kerins (2004). This model, providing remarkable good fits to the

M31 surface brightness and rotation curve profiles, can be considered as an acceptable model for the mass distribution in the M31 galaxy. Accordingly, the mass density of the M31 disk stars is described by a sech-squared profile

$$\rho_D(R, z) = \rho_D(0) \exp(-R/h) \operatorname{sech}^2(z/H), \quad (19)$$

where $H = 0.3$ kpc, $h = 6.4$ kpc and $\rho_D(0) = 0.35 \times 10^9 M_\odot \text{pc}^{-3}$ are, respectively, the scale height and scale lengths of the disk and the disk central mass density. R is the distance on the M31 disk plane (described by the coordinates x and y) and z is the distance from it. The M31 disk is assumed to be inclined by an angle $i = 77^\circ$ and the azimuthal angle relative to the near minor axis is $\phi = -38.6^\circ$.

The M31 bulge is parameterized by a flattened power law of the form

$$\rho_B(R, z) = \rho_B(0) \left[1 + \left(\frac{R}{\tilde{a}} \right)^2 + q^{-2} \left(\frac{z}{\tilde{a}} \right)^2 \right]^{-s/2}, \quad (20)$$

where $\rho_B(0) \simeq 4.5 \times 10^9 M_\odot \text{kpc}^{-3}$, $q \simeq 0.6$ is the ratio of the minor to major axis, $\tilde{a} \simeq 1$ kpc and $s \simeq 3.8$. Both the M31 disk and bulge are truncated at a distance $R = 40$ kpc.

We remark that the twisting of the optical isophotes in the inner M31 regions indicates that the bulge major axis is offset by $\simeq 15^\circ$ from the disk major axis (Stark and Binney, 1994). The consideration of this effect by Kerins et al. 2005 leads to the evaluation of pixel lensing rates that show spatial distributions tilted of the same amount inside 5 arcmin from the M31 center. The twisting effect vanishes at larger distances due to the increasing contribution to microlensing by M31 disk and halo. Clearly, our results in Figs. 1-3 do not show the above mentioned effect since here we are considering only a flattened bulge without twist. However, we expect that the consideration of the isophote twisting does not substantially modify our results about both MACHO-to-self lensing probability and event time scale ratios (given in Tabs. 2-5), particularly for events at large distance from the M31 center.

The dark matter in the M31 halo is assumed to follow an isothermal profile

$$\rho_H(r) = \rho_H(0) \frac{a^2}{a^2 + r^2}, \quad (21)$$

with core radius $a = 4$ kpc and central dark matter density $\rho_H(0) = 6.5 \times 10^7 M_\odot \text{kpc}^{-3}$. The M31 halo is truncated at 100 kpc with asymptotic rotational velocity $v_{rot} \simeq 235$ km s^{-1} .

We do not consider other dark matter distribution models, as King-Michie (Binney and Tremaine, 1987) or NFW (Navarro et al., 1997) suggested by N body simulations. The effect of using such models, which have a more concentrated dark mass distribution, is both to decrease the spatial distribution of MACHOs at large distance from the M31 center, where the rotation curve is poorly determined, and to increase it in the innermost region, where

the MACHO contribution is relatively unimportant with respect to that of bulge and disk. Regarding the former aspect, we also note that in the MEGA experiment the typical MACHO lens distance (about 20 kpc) is too small to appreciate the effect of this choice. Overall, the current data do not allow one to perform a meaningfully fine tuning of the dark matter parameters.

As usual, the mass density profile for the MW disk is described with a double exponential profile

$$\rho_D(R, z) = \rho_D(R_0) \exp(-(R - R_0)/h) \exp(-|z|/H), \quad (22)$$

with Earth position from the Galactic center at $R_0 \simeq 8.5$ kpc, scale height $H \simeq 0.3$ kpc, scale length $h \simeq 3.5$ kpc and local mass density $\rho_D(R_0) \simeq 1.67 \times 10^8 M_\odot \text{ kpc}^{-3}$.

The dark halo in our Galaxy is also assumed to follow an isothermal profile with core radius $a \simeq 5.6$ kpc and local dark matter density $\rho_H(R_0) \simeq 1.09 \times 10^7 M_\odot \text{ kpc}^{-3}$. The corresponding asymptotic rotational velocity is $v_{rot} \simeq 220 \text{ km s}^{-1}$. The MW halo is truncated at $R \simeq 100$ kpc.

For both M31 and MW halos, the fraction of dark matter in form of MACHOs is assumed to be $f_h \simeq 0.2$ (Alcock et al., 2000). However, most of our results can easily be rescaled to get the corresponding figures for other values of f_{MACHO} .

Moreover, we assume that the random velocities of stars and MACHOs follow Maxwellian distributions with one-dimensional velocity dispersion $\sigma = 30, 100, 166 \text{ km s}^{-1}$ and $30, 156 \text{ km s}^{-1}$ for the M31 disk, bulge, halo and MW disk and halo, respectively. In addition, a M31 bulge rotational velocity of 30 km s^{-1} has been taken into account (Kerins et al., 2001; An et al., 2004).

3.2. Stellar luminosity function

Pixel lensing event detection by the MEGA collaboration is performed in the red band¹ and, thus, red giants are the most luminous stars in this band. Therefore, we may safely assume that the overwhelming majority of the pixel lensing event sources are red giants.

Moreover, in the lack of precise information about the stellar luminosity function in M31, we adopt the luminosity function derived from the stars in the Galaxy and assume that it also holds for M31.

Accordingly, following (Mamon and Soneira, 1982) we assume that the stellar luminosity function does not depend on the position and in the magnitude range $-6 \leq M \leq 16$ it is proportional to the expression

$$\phi_*(M) \propto \frac{10^{\beta(M-M^*)}}{[1 + 10^{-(\alpha-\beta)\delta(M-M^*)}]^{1/\delta}}, \quad (23)$$

where, in the red band, $M^* = 1.4$, $\alpha \simeq 0.74$, $\beta = 0.045$ and $\delta = 1/3$. Moreover, the fraction of red giants (over the

¹ Indeed, observations in the red band, by minimizing light absorption in M31 and MW disks by the intervening dust, offer the best compromise between sampling and sky background. Observations in other bands (B and V) are commonly used to test achromaticity of the candidate events.

total star number) as a function of M is approximated as (Mamon and Soneira, 1982)

$$f_{RG}(M) = \begin{cases} 1 - C \exp[\alpha(M + \beta)^\gamma] & \text{for } -6 \leq M \leq 3 \\ 0 & \text{for } M \geq 3, \end{cases} \quad (24)$$

where, in the red band, $C \simeq 0.31$, $\alpha \simeq 6.5 \times 10^{-4}$, $\beta = 7.5$ and $\gamma \simeq 3.2$.

Therefore, the red giant luminosity function will be $\phi_{RG}(M) \propto \phi_*(M) \times f_{RG}(M)$ and the fraction of red giants averaged on the magnitude is given by

$$\langle f_{RG} \rangle = \frac{\int_{-6}^3 \phi_{RG}(M) dM}{\int_{-6}^{16} \phi_*(M) dM} \simeq 5.3 \times 10^{-3}, \quad (25)$$

from which it follows that the local number density of red giants will be $n_{RG} \simeq 5.3 \times 10^{-3} n_*$, where n_* is the local stellar number density.

3.3. Mass functions

As concerns the lens mass function $\psi_0(\mu)$ in eqs. (8) - (11), for lenses belonging to the bulge and disk star populations, the lens mass is assumed to follow a broken power law (Gould et al., 1997)

$$\psi_0(\mu) = \begin{cases} K \mu^{-0.56} & \text{for } 0.1 \leq \mu \leq 0.59 \\ K \mu^{-2.20} & \text{for } 0.59 \leq \mu \leq \mu_{up} \end{cases} \quad (26)$$

where the lower limit $\mu_{min} = 0.1$ and the upper limit μ_{up} is 1 for M31 bulge stars and 10 for M31 and MW disk stars (see also Kerins et al., 2001). K is fixed according to the normalization given by eq. (9). The resulting mean mass for lenses in the bulges and disks are $\langle m_b \rangle \sim 0.37 M_\odot$ and $\langle m_d \rangle \sim 0.69 M_\odot$, respectively.

For the lens mass in the M31 and MW halos we assume the δ -function approximation

$$\psi_0(\mu) = \frac{\rho_0}{M_\odot \mu_h} \delta(\mu - \mu_h) \quad (27)$$

and we take a MACHO mass, in solar units, $\mu_h = 10^{-2}, 10^{-1}, 0.5, 1$.

4. Analytical results

In the present analysis we adopt the parameters for the INT and the Sloan-r filter on the WFC (Wide-Field Camera) used by the MEGA collaboration (de Jong et al., 2004). The Telescope diameter, the pixel field of view and the image exposition time are 2.5 m, 0.33 arcsec and $t_{exp} = 760$ s, respectively. We also use a gain or conversion factor of $2.8 \text{ e}^-/\text{ADU}$, and a loss factor $\simeq 3$, for both atmospheric and instrumental. The zero-point with the Sloan-r WFC turns out to be $\sim 24.3 \text{ mag arcsec}^{-2}$ (Belokurov et al., 2005). Moreover, we adopt a value $\simeq 1.5$ arcsec for the average seeing conditions, a sky background $m_{sky} \simeq 20.9 \text{ mag arcsec}^{-2}$ (corresponding to a Moon eclipse) and a minimum noise level of $\sim 2.5 \times 10^{-3} N_{bl}$. N_{bl} is the baseline photon count which is the sum of the

M31 surface brightness given by Kent (1989) and the sky contribution.

Maps of optical depth, expected event number and event timescale in pixel lensing experiments have been presented in a previous paper (De Paolis et al., 2005) together with the study of the dependence on microlensing quantities with the assumed M31 mass distribution model (see also Kerins 2004). Our results are also in good agreement with previous analytical estimates for the rate, the timescale distribution and the optical depth (Baltz et al., 2003; Gyuk and Crotts, 2000).

In Fig. 1 the map of $\langle u_T(x, y) \rangle_{\phi_{RG}}$ shows that in the central M31 regions the lens impact parameter on average is ≤ 0.04 implying that only high magnified events with $A_T \geq 25$ are in principle detectable. The asymmetrical shape is due to the internal extinction of the M31 disk for which we use the value 0.74 mag given by Kent (1989). Indeed, due to the inclination of the M31 disk, along a line of sight towards the southern region there exists a larger number of source stars (with respect to the corresponding northern field) which are not absorbed by the M31 disk dust (and therefore appear with a smaller magnitude), lying at larger averaged values for u_T .

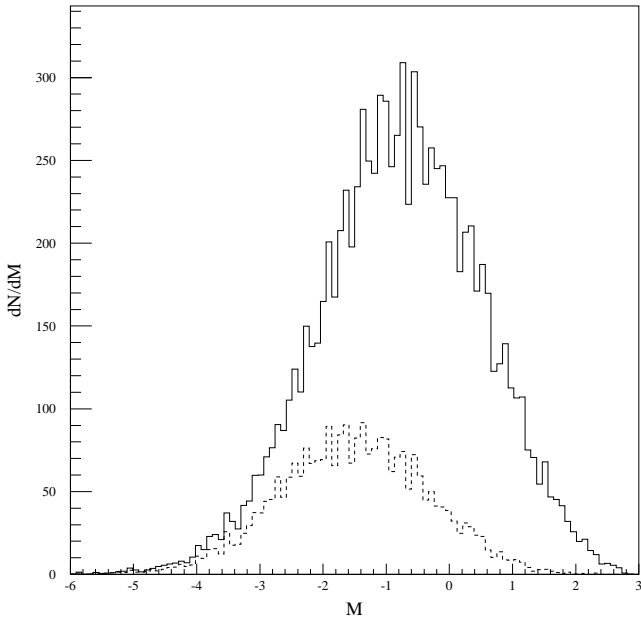


Fig. 4. Plot of the source absolute magnitude distribution for the generated events (solid line) and for the revealed events (dashed line) towards the MEGA 7 direction.

In Fig. 2, assuming a MACHO mass $\mu_h = 0.5$ and a halo MACHO fraction $f_h = 0.2$, we show the map of the MACHO-to-self lensing probability ratio $(P_h/P_s)_{An}$. We find that in the M31 central regions microlensing is dominated by self-lensing contributions while MACHO-lensing becomes important at distances > 10 arcmin from the center. In the figure it is also evident the well known

Table 2. MACHO-to-self lensing probability ratio $(P_h/P_s)_{An}$ towards the 14 MEGA events are given for different MACHO mass values.

MEGA	$\mu_h = 0.01$	0.1	0.5	1
1	1.65	0.52	0.23	0.16
2	1.76	0.56	0.25	0.18
3	2.22	0.71	0.31	0.22
4	2.52	0.78	0.35	0.24
5	24.58	7.72	3.46	2.40
6	23.46	7.53	3.38	2.40
7	12.93	3.83	1.80	1.26
8	9.79	3.15	1.40	0.96
9	19.49	6.15	2.79	1.99
10	17.19	5.44	2.42	1.73
11	19.22	6.04	2.74	1.88
12	18.91	5.88	2.62	1.91
13	54.13	17.60	7.87	5.67
14	112.32	35.47	17.07	11.12

Table 3. MACHO-to-self lensing Einstein time ratio $\langle t_{Eh} \rangle / \langle t_{Es} \rangle$ towards the 14 MEGA events are given for different MACHO mass values.

MEGA	$\mu_h = 0.01$	0.1	0.5	1
1	0.30	0.96	2.15	3.02
2	0.31	1.00	2.42	3.24
3	0.29	0.94	2.02	2.91
4	0.20	0.65	1.47	2.12
5	0.16	0.51	1.10	1.59
6	0.16	0.49	1.09	1.55
7	0.15	0.52	1.10	1.58
8	0.13	0.41	0.92	1.35
9	0.13	0.42	0.97	1.34
10	0.17	0.54	1.21	1.69
11	0.16	0.50	1.11	1.61
12	0.14	0.44	0.98	1.36
13	0.16	0.49	1.08	1.51
14	0.15	0.48	1.03	1.52

near-far disk asymmetry due to the inclination of the M31 disk (Crotts, 1992; Baillon et al., 1993; Jetzer, 1994).

In Tab. 2, we show how the MACHO-to-self lensing probability ratio $(P_h/P_s)_{An}$ depends on the MACHO mass μ_h towards the 14 MEGA events. The general trend is that $(P_h/P_s)_{An}$ increases as μ_h decreases as a consequence of the increase of the MACHO number density. Moreover, for a given value of μ_h , $(P_h/P_s)_{An}$ increases with the distance from the M31 center.

In Fig. 3 the map of the MACHO-to-self lensing Einstein time ratio $(t_{Eh}/t_{Es})_{An}$ is given for a MACHO mass of $0.5 M_\odot$. In the region inside $\simeq 5$ arcmin from the M31 center microlensing events due to MACHOs have twice as long a duration as compared to self-lensing events, while in the regions far away from the M31 center all events have roughly the same duration. Obviously, the MACHO-to-self lensing Einstein time ratio depends on the assumed MACHO mass. This fact is clearly seen in Tab. 3, where the ratio $(\langle t_{Eh} \rangle / \langle t_{Es} \rangle)_{An}$ towards the

14 MEGA events is given for different MACHO mass values. $\mu_h = 0.5$ corresponds to the MACHO mass value for which the 10 outer MEGA events (5-14) are characterized by having a MACHO-to-self lensing Einstein time ratio equal to unity, i.e., events due to either MACHO-lensing or self-lensing have roughly the same duration. Thus, these different types of events are indistinguishable on the basis of their timescale alone. The situation is instead much more favorable for MACHO masses smaller or larger than $0.5 M_\odot$.

We would like to emphasize that in pixel lensing experiments t_E is not a directly observable quantity, since the relevant time scale is the full-width half-maximum event duration $t_{1/2}$, which depends on t_E and the impact parameter u_0 (Gondolo, 1999). However, since the probability for a given u_0 value is practically the same for self-lensing and MACHO-lensing events (as we have verified by using the MC code) the ratio $(\langle t_{E h} \rangle / \langle t_{E s} \rangle)_{An}$ is equivalent to the ratio $(\langle t_{1/2 h} \rangle / \langle t_{1/2 s} \rangle)_{An}$, at least for the MC generated events. Of course, as it will be more clear in the following Sections (in particular from Tab. 4 and Fig. 10), it does not mean that the same conclusion holds for the MC revealed events, since the (normalized) event number which pass the MEGA selection criteria turns out to depend on $t_{1/2}$ and R_{max} (see Fig. 6).

5. Monte Carlo simulation

Once the event location (one of the 14 MEGA events towards M31) has been selected, for any lens and source population present along the line of sight we have to make as next the choice over the following five parameters: source distance D_{os} , lens distance D_{ol} , lense effective transverse velocity $v_{1\perp}$, lens mass μ and source magnitude M . We shall denote these parameters by x_i , with $i = 1, \dots, 5$ in the order just listed (e.g. $x_1 = D_{os}$, etc.). The probability with which we select the events according to one of the parameters is then given by

$$P(x_i)dx_i = \frac{1}{N_{ev}} \frac{\partial N_{ev}}{\partial x_i} dx_i \quad (28)$$

where $\frac{\partial N_{ev}}{\partial x_i}$ is defined as being the integrand of the event number N_{ev} integrated over all variables x_j without, however, the considered variable x_i . Clearly when integrating $\frac{\partial N_{ev}}{\partial x_i}$ over dx_i we obtain again N_{ev} .

This way, for instance, for self-lensing events the probability of extracting a lens with mass μ turns out to be

$$P(x_4 = \mu)d\mu \propto \mu^{1/2} \psi_0(\mu)d\mu, \quad (29)$$

where $\psi_0(\mu)$ is the lens number density distribution defined in eq. (26).

The probability of a source² at distance D_{os} and a lens at distance D_{ol} from the observer, respectively, is given by

$$P(D_{os})dD_{os} \propto \rho_s(D_{os})D_{os}^{3/2} \left(\int_0^{D_{os}} P(D_{ol})dD_{ol} \right) dD_{os} \quad (30)$$

² Here we take into account that the source number inside the pixel solid angle increases with the distance as D_{os}^2 .

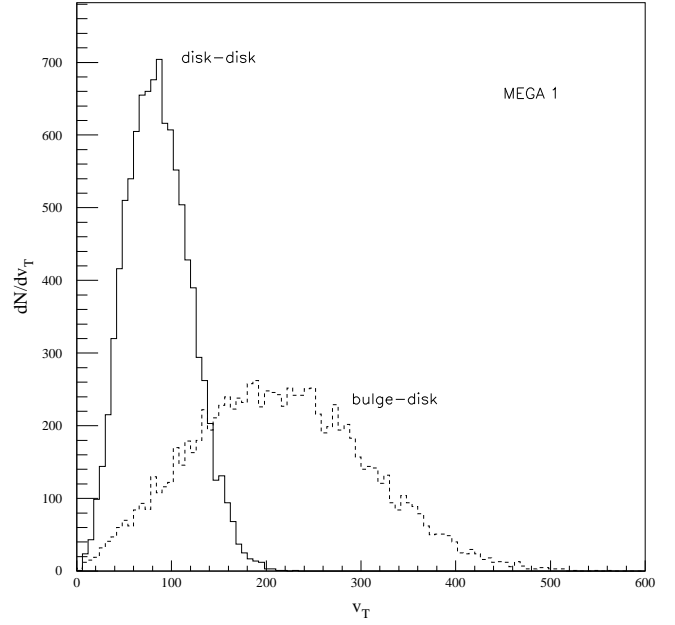


Fig. 5. The lens transverse velocity $v_{1\perp}$ distribution for the MC generated events towards the MEGA 1 direction is shown in the case of disk-disk (solid line) and bulge-disk events (dashed line).

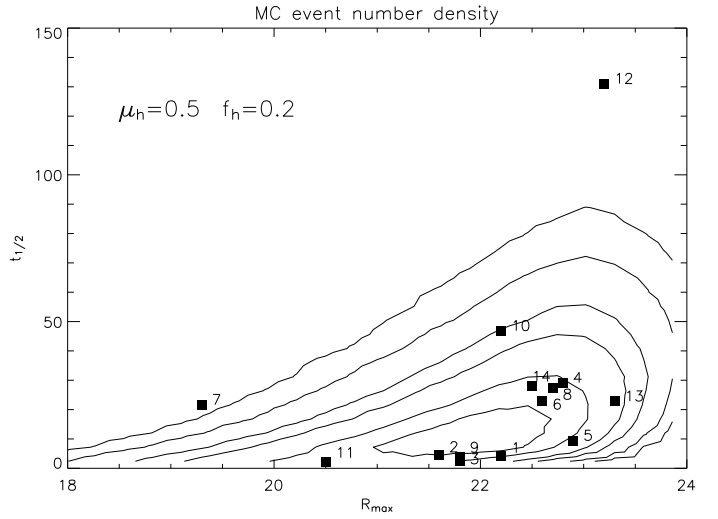


Fig. 6. MC revealed event number density \mathcal{N}_{ev}^{rev} plot (normalized to the maximum value) as a function of $t_{1/2}$ and R_{max} . Here we consider both self-lensing and MACHO-lensing events, averaged over all the 14 MEGA directions and we assume $\mu_h = 0.5$ and $f_h = 0.2$. From the inner to the outer part \mathcal{N}_{ev}^{rev} decreases with lines referring to values 0.7, 0.5, 0.3, 0.2, 0.1, 0.05.

and

$$P(D_{ol})dD_{ol} \propto \rho_l[D_{ol}(D_{os} - D_{ol})]^{1/2}(D_{ol}) dD_{ol}, \quad (31)$$

where $\rho_l(D_{ol})$ and $\rho_s(D_{os})$ are, respectively, the lens and the source mass densities.

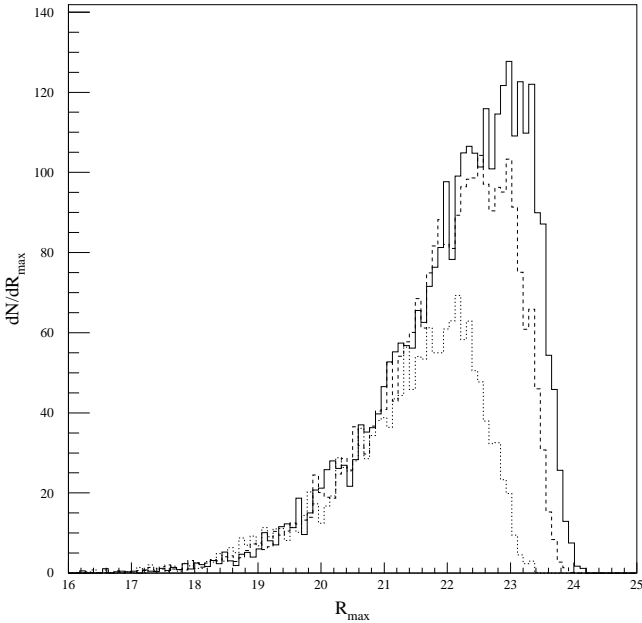


Fig. 7. The R_{\max} distribution for the MC revealed events towards the MEGA 14 (solid line), 7 (dashed line) and 1 (dotted line) directions.

The probability of extracting a source with magnitude M is weighted by the function

$$P(M)dM \propto u_T(M)\phi_{RG}(M)dM, \quad (32)$$

where $\phi_{RG}(M)$ is the source magnitude distribution for red giants defined by means of eqs. (23) - (24) and, through $u_T(M)$, we take into account the surface brightness variation along the field of view. Indeed, we find that the median value of the source magnitude distribution decreases from $M^{\text{median}} = -2.18$ for the innermost MEGA directions to $M^{\text{median}} = -1.18$ for the outermost ones. In Fig. 4 we show the distribution of the source absolute magnitude for all MC generated events and for the revealed (see after) events towards the direction of the MEGA 7 event. For a given source and lens position the probability of extracting a lens with transverse velocity v_{\perp} is given by eq. (12), where $z = v_{\perp}/\sigma_1$. In Fig. 5, for both disk-disk and bulge-disk events, we show the lens transverse velocity distributions for MC generated events towards the MEGA 1 direction. The shorter $\langle v_{\perp} \rangle$ value in the first case will lead to an increase in the event timescale.

The probability of extracting an event with impact parameter $x_5 = u_0$ is constant for values of u_0 in the interval in between 0 and u_T , as defined in eq. (17)³. Thus it is assumed that

$$P(u_0) \propto \text{const.} \quad (33)$$

³ In order to avoid a sharp cutoff in several obtained plots (see, e.g., Fig. 7) we allow for events with $u_0 \gtrsim u_T$ to be detected.

Once all the parameters have been fixed, for each event we build the corresponding lightcurve using the same time sampling of the MEGA campaign and the same observing and instrumental conditions of the considered experiment. We add a gaussian noise modulated by the Moon phase and use a Paczyński fit (Paczynski, 1986) to evaluate the microlensing parameters.

The selection of the MC generated events is based on the same criteria adopted by the MEGA collaboration. By using the results of the Paczyński fit we filter the lightcurves with the following selection criteria: *peak sampling*, *peak significance*, *peak width*, *baseline flatness* and *goodness of fit* (for more details see Appendix A.1 in de Jong et al. 2004). The criteria that more severely cut the MC generated events are the *peak sampling* and the *peak significance*, which depends through the evaluation of the statistical errors on the the Moon phase. The former criterium leads to select events with well sampled lightcurves (within the MEGA campaign), the latter to events with high signal-to-noise ratios. The fraction of MC selected events also depends on the event location through the threshold value of R_{\max} . This effect is further discussed in the following section.

6. Monte Carlo results

MC results allow to estimate the features of the revealed events which pass the adopted selection criteria. In Fig. 6, assuming a MACHO mass $\mu_h = 0.5$ and a halo MACHO fraction $f_h = 0.2$ we give the contour plot, in the $(t_{1/2}, R_{\max})$ parameter space, of the event number density

$$\mathcal{N}_{\text{ev}}^{\text{rev}} = \frac{d^2 N_{\text{ev}}^{\text{rev}}}{dt_{1/2} dR_{\max}}, \quad (34)$$

averaged on all the 14 MEGA directions, for both self-lensing and MACHO-lensing events. We also give in the same parameter space the position of the 14 observed MEGA events. $\mathcal{N}_{\text{ev}}^{\text{rev}}$ is maximum in the region $t_{1/2} \simeq 20$ day and $R_{\max} \simeq 22$. Moreover, $\mathcal{N}_{\text{ev}}^{\text{rev}}$ rapidly decreases for $R_{\max} > 23.5$ (due to the lack of revealed events with low signal-to-noise ratio) and $t_{1/2} < 5$ day (due to the peak sampling) and in the region of high amplification and long duration events (upper-left region of the figure), due to the absence of MC generated events. Actually, the last cutoff depends on the adopted MACHO mass value and shifts towards smaller $t_{1/2}$ values decreasing μ_h . Indeed, in Fig. 6 the crucial parameter determining the event distribution is the lens mass value and it turns out that the region where $\mathcal{N}_{\text{ev}}^{\text{rev}}$ is maximum scales with μ_h in the same way as $t_{1/2}^{\text{median}}$ and R_{\max}^{median} (see Tab. 4, where we give the median values of the distributions of the MC revealed events as a function of the lens star mass μ_* , $t_{1/2}$ and R_{\max}).

From Tab. 4 for $\mu_h = 0.5$ one can infer that the $\mathcal{N}_{\text{ev}}^{\text{rev}}$ plot does not vary substantially for MACHO-lensing and self-lensing events occurring away from the M31 center, since the lens stellar mass is of the same order of the

Table 4. For the MC revealed events (which pass the MEGA selection criteria), the median values μ_*^{median} (column 2) of the lens star mass distribution for self-lensing events, $t_{1/2}^{\text{median}}$ (columns 3-7) and $R_{\text{max}}^{\text{median}}$ (columns 8-12) for self-lensing and MACHO-lensing are given towards the 14 MEGA events.

MEGA	μ_*^{median}	$t_{1/2}^{\text{median}}$					$R_{\text{max}}^{\text{median}}$				
	self	self	MACHO				self	MACHO			
		$\mu_h = 0.01$	0.1	0.5	1	$\mu_h = 0.01$	0.1	0.5	1		
1	0.48	15.66	4.96	11.22	19.51	22.49	21.56	21.16	21.45	21.65	21.61
2	0.48	15.33	5.06	11.22	18.15	22.04	21.62	21.31	21.52	21.64	21.70
3	0.49	16.38	5.17	11.20	19.32	22.62	21.69	21.41	21.64	21.76	21.74
4	0.62	18.16	5.04	11.43	18.81	23.04	21.87	21.57	21.85	21.93	21.94
5	0.46	20.62	4.85	11.43	19.80	23.59	22.22	21.85	22.11	22.23	22.22
6	0.46	21.43	4.77	11.57	19.88	24.27	22.17	21.85	22.11	22.23	22.23
7	0.50	20.72	4.95	10.97	19.12	22.96	22.10	21.79	22.02	22.14	22.19
8	0.65	21.47	5.15	11.60	19.90	23.65	22.13	21.81	22.05	22.18	22.21
9	0.57	24.04	5.20	12.21	19.94	24.17	22.19	21.85	22.08	22.18	22.20
10	0.45	20.07	4.73	10.79	18.98	23.09	22.19	21.83	22.06	22.20	22.24
11	0.46	20.37	4.88	11.02	19.79	23.66	22.14	21.86	22.08	22.21	22.22
12	0.52	22.30	5.00	11.77	20.24	23.94	22.17	21.84	22.05	22.20	22.21
13	0.44	22.58	4.98	12.24	21.14	25.28	22.32	21.99	22.20	22.34	22.35
14	0.43	24.15	5.34	12.58	21.90	26.53	22.34	22.03	22.25	22.35	22.38

Table 5. MACHO-to-self lensing probability ratios $(P_h/P_s)_{\text{MC}}$ towards the 14 observed MEGA events are given for different MACHO mass values. Probabilities are now calculated from eq. (35) by considering microlensing rates, $t_{1/2}$ and R_{max} distributions for the MC revealed events. The results in the table scale with the MACHO fraction value as $f_h/0.2$.

MEGA	$\mu_h = 0.01$	0.1	0.5	1
1	3.65	0.70	0.18	0.10
2	5.71	0.79	0.16	0.08
3	6.70	1.06	0.23	0.14
4	0.36	0.56	0.33	0.24
5	63.51	13.41	3.64	1.98
6	7.56	6.56	3.48	2.35
7	0.45	1.83	1.46	3.04
8	2.67	2.88	1.46	0.97
9	109.47	14.32	3.58	1.74
10	0.98	1.95	1.98	1.79
11	62.95	8.29	2.56	1.28
12	0.04	0.55	1.36	1.79
13	20.81	23.20	9.44	4.98
14	26.99	29.88	18.50	12.24

MACHO mass. Moreover, for any value of μ_h , the $\mathcal{N}_{\text{ev}}^{\text{rev}}$ distribution is also weakly dependent on the selected direction towards M31. The situation is completely different for $\mu_h \neq 0.5$, and this means that self-lensing and MACHO-lensing events lie on different regions in the $(t_{1/2}, R_{\text{max}})$ parameter space of the corresponding $\mathcal{N}_{\text{ev}}^{\text{rev}}$ plot.

The dependence of $t_{1/2}^{\text{median}}$ and $R_{\text{max}}^{\text{median}}$ on the lens mass and the MEGA direction is also clear from Tab. 4. For self-lensing events, $t_{1/2}^{\text{median}}$ increases from the inner to the outer part of the M31 galaxy, and in this region $t_{1/2}^{\text{median}}$ also increases for increasing values of μ_*^{median} , following the dependence of the Einstein radius with the

lens mass⁴. Moreover, for MACHO-lensing events with a fixed μ_h value, $t_{1/2}^{\text{median}}$ is almost the same for any MEGA direction, while it increases, as expected, with the lens mass.

In Tab. 4 is also evident the decrease, moving towards the M31 center, of the $R_{\text{max}}^{\text{median}}$ value that follows the surface brightness variation along the field. In particular, we find a shift of about 1 mag going from the inner to the outer regions. In Fig. 7 we give the (revealed) event distributions as a function of R_{max} towards the MEGA 1, 7 and 14 directions. This clearly shows how the event location affects the fraction of the revealed events.

The event distributions as a function of $t_{1/2}$, for both self-lensing (solid line) and MACHO-lensing (dashed line) revealed events are shown in Fig. 8, for $\mu_h = 0.5$ and for the 1 and 7 MEGA directions towards M31 (representative of inner and outer events, respectively). Only in the case of the MEGA 1 direction the obtained distributions are markedly different for self-lensing and MACHO-lensing, since self-lensing events are shorter than MACHO-lensing events. For the MEGA 7 direction (and the other outer directions) self-lensing and MACHO lensing with the same lens mean mass have roughly the same $t_{1/2}$ distributions.

Our MC results can be used to estimate the lens nature and location of the 14 MEGA candidate events, by weighting the microlensing rate - giving the analytical estimates of the MACHO-to-self lensing probability ratio $(P_h/P_s)_{\text{An}}$ shown in Tab. 2 - with the revealed event number density distribution and taking also into account the observed features of the MEGA events. In Tab. 5, assuming a halo MACHO fraction $f_h = 0.2$ and different MACHO mass

⁴ For self-lensing events, the lens median mass value changes with the MEGA direction, since the disk lens mass is on average higher than the bulge lens mass and the disk-to-bulge probability ratio depends on the MEGA direction.

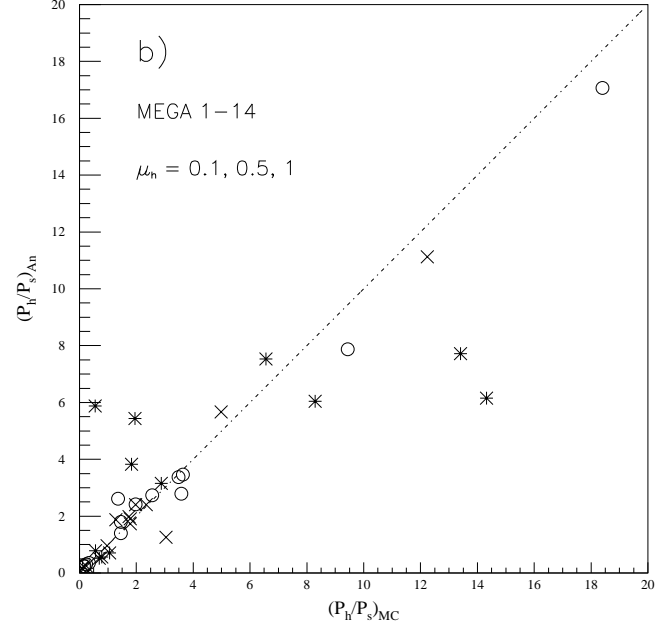
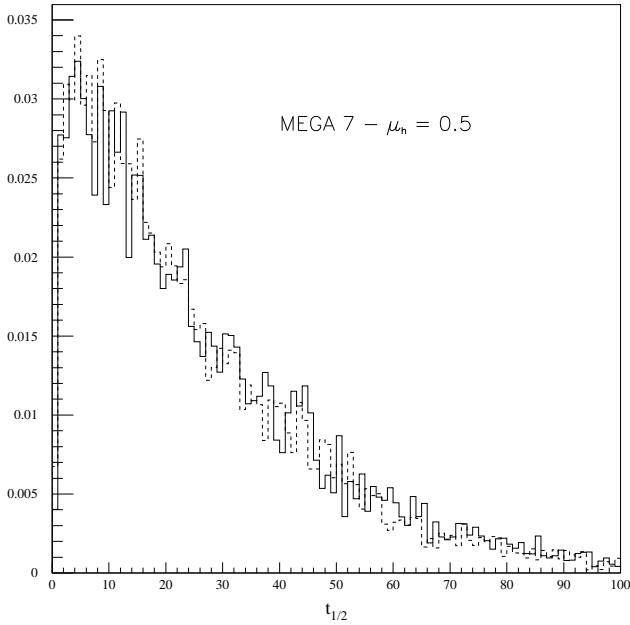
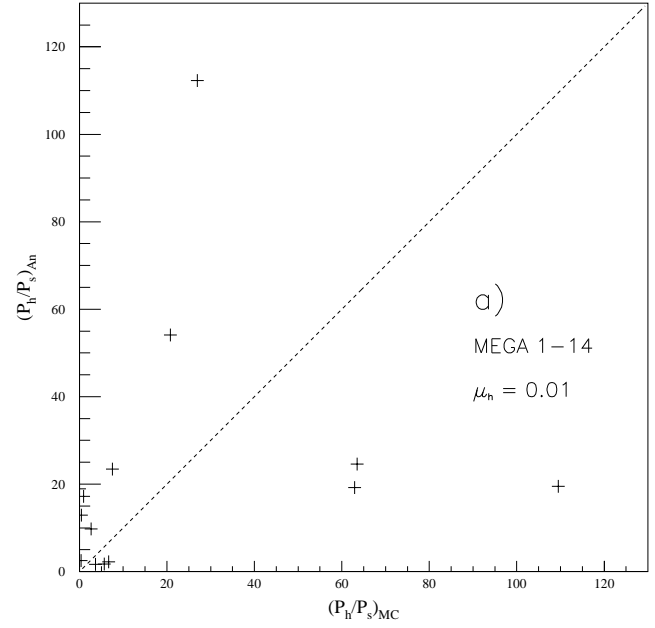
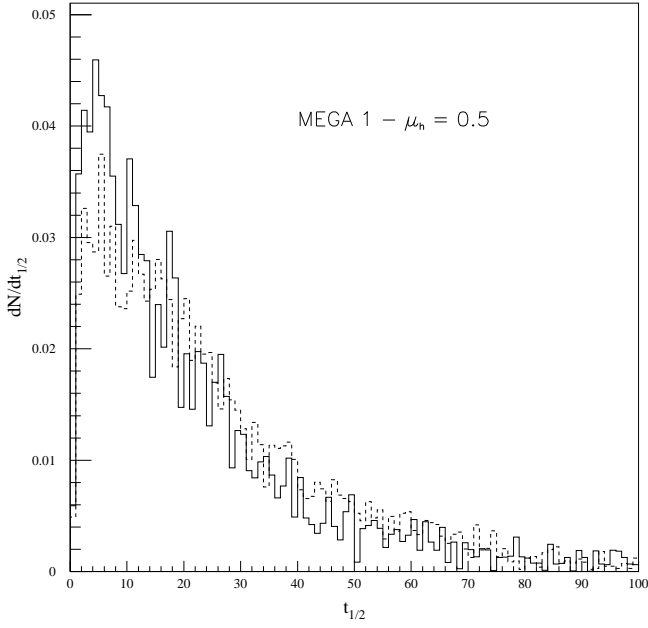


Fig. 8. The $t_{1/2}$ distributions are shown for MEGA 1 and 7 events and for $\mu_h = 0.5$. In each panel, the solid curve refers to self-lensing events and the dashed curve to MACHO-lensing events.

values, we give the MC MACHO-to-self lensing probability ratio

$$\left(\frac{P_h}{P_s}\right)_{MC} = \left(\frac{P_h}{P_s}\right)_{An} \frac{\mathcal{N}_{ev\ h}^{rev}(t_{1/2}^{obs}) \mathcal{N}_{ev\ h}^{rev}(R_{max}^{obs})}{\mathcal{N}_{ev\ s}^{rev}(t_{1/2}^{obs}) \mathcal{N}_{ev\ s}^{rev}(R_{max}^{obs})} \quad (35)$$

where we indicate with $\mathcal{N}_{ev}^{rev}(t_{1/2}^{obs})$ and $\mathcal{N}_{ev}^{rev}(R_{max}^{obs})$ the number of events (either MACHO or self-lensing) with du-

Fig. 9. Plot of $(P_h/P_s)_{An}$ versus $(P_h/P_s)_{MC}$ for all the 14 MEGA events. In panel a) we consider a MACHO mass $\mu_h = 0.01$ and we use the symbol plus; in panel b) we take $\mu_h = 0.1, 0.5, 1$ and use symbols time, circle, asterisk, respectively.

ration and magnitude at maximum, respectively, within 2 standard deviations around the observed values. Here, we remark that each \mathcal{N}_{ev} distribution is normalized to the total number of revealed events. A comparison between the analytical and MC results given, respectively, in Tabs. 2 and 5 is presented in Figs. 9a and 9b, where we plot

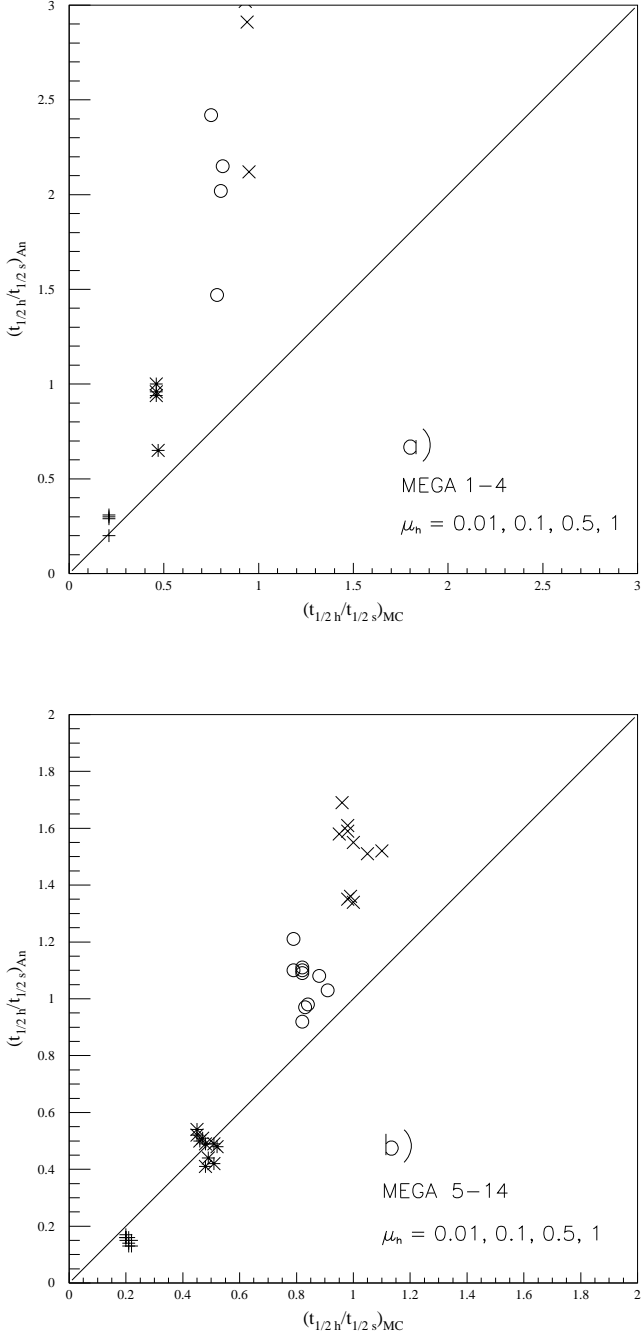


Fig. 10. Plot of $(t_{1/2 h}/t_{1/2 s})_{An}$ versus $(t_{1/2 h}/t_{1/2 s})_{MC}$, for $\mu_h = 0.01, 0.1, 0.5, 1$. The symbols are as in Fig. 9. In panel a) we consider MEGA 1-4 and in panel b) MEGA 5-14 events, respectively.

$(P_h/P_s)_{An}$ versus $(P_h/P_s)_{MC}$, for the MACHO mass values $\mu_h = 0.01$ and $\mu_h = 0.1, 0.5, 1$, respectively. Only for $\mu_h = 0.5$ and for the outer events MC and analytical estimates are in good agreement, since, as we have already discussed above, MACHO-lensing and self-lensing events have for this particular mass value, on average, the same features.

Also for the time scale ratios between MACHO-lensing and self-lensing events analytical and MC results give different estimates. A comparison of the analytical results in Tab. 3 and MC results in Tab. 4 is presented in Figs. 10a and 10b, where we show $(t_{1/2 h}/t_{1/2 s})_{An}$ versus $(t_{1/2 h}/t_{1/2 s})_{MC}$ for MEGA 1-4 and 5-14 events. The difference is particularly important for the events 1-4.

It emerges, therefore, clearly that the MC analysis is essential for determining the lens nature and location of microlensing events, at least if the MACHO mass differs substantially from the average self-lensing mass. From Tab. 5, we find that MEGA events 1-4 are most likely self-lensing events for MACHO masses greater than 0.1 solar masses, while events 5, 6, 9, 11, 13, 14 are likely MACHO-lensing. For the other MEGA directions the lens nature is more uncertain. As a final comment on Fig. 6, we note that the event 12, lying in a region of low (revealed) event number density, hardly can be considered a reliable microlensing event, unless the MACHO mass is considerably greater than $1 M_\odot$.

7. Conclusions

We have studied the main features of the expected microlensing events in pixel lensing observations towards M31, by using both analytical estimates (from the microlensing rate) as well as results by a MC code where we reproduce the observing and instrumental conditions of the MEGA experiment.

First of all, we derive in Section 2 the microlensing rate, and assuming a specific mass distribution model for M31 and the Galaxy, we calculate the MACHO-to-self lensing probability and the MACHO-to-self lensing event time scale ratios. For $\mu_h > 0.1$, we find that self-lensing dominates in the M31 central regions. Moreover, for $\mu_h \simeq 0.5$, towards the innermost MEGA directions, MACHOs events have duration twice as long as self-lensing events, while outer events have roughly the same duration.

We then generate a large number of MC microlensing events by choosing relevant source and lens parameters as outlined in Section 5. We study the observability of the MC events, by considering the capabilities of the INT Telescope, typical observing conditions and the event selection criteria adopted by the MEGA Collaboration.

MC results can be used to evaluate, for the 14 MEGA candidate events, the MACHO-to-self lensing probability and the event time scale ratios $(P_h/P_s)_{MC}$ and $(t_{1/2 h}/t_{1/2 s})_{MC}$ (given in Tabs. 4 and 5), by taking into account not only the analytical expectations from the microlensing rate (as already done in Tabs. 2 and 3) but also the features of the MC (revealed) events and the observed values of $t_{1/2}$ and R_{max} . MC results and analytical expectations are compared in Figs. 9 and 10, where one can see that in determining the lens nature and location of the MEGA candidate events, the MC analysis is particularly important for $\mu_h \neq 0.5$. Accordingly, we find that event 12, lying in a region of low event number density,

hardly can be considered a reliable microlensing event, unless the MACHO mass is considerably larger than $1 M_{\odot}$. Moreover, for a MACHO mass greater than $0.1 M_{\odot}$, the innermost MEGA events 1, 2, 3, 4 are most likely self-lensing events, while 5, 6, 9, 11, 13, 14 are MACHO-lensing events. For the other MEGA directions the lens nature is more uncertain.

Acknowledgements. SCN is supported by the Swiss National Science Foundation.

References

- Alcock C., Akerloff C. W., Allsman R. A. et al. , 1993, *Nat.*, 365, 621.
- Alcock C., Allsman R. A., Alves D. R. et al. , 2000, *ApJ*, 542, 281.
- An J. H., Evans N. W., Kerins E. et al., 2004, *ApJ*, 601, 845.
- Ansari R., Auriere M., Baillon P. et al., 1997, *A&A*, 324, 843.
- Aubourg E., Bareyre P., Brehin S. et al. , 1993, *Nat.*, 365, 623.
- Baillon P., Bouquet A., Giraud-Heraud Y. & Kaplan J., 1993, *A&A*, 277, 1.
- Baltz E. A., Gyuk G. & Crofts A. P. S., 2003, *ApJ*, 582, 30.
- Belokurov V., An. J., Evans N.W. et al., 2005, *MNRAS*, 357, 17.
- Binney J. & Tremaine S., 1987, *Galactic Dynamics*, Princeton University Press, Princeton, New Jersey.
- Calchi Novati S., Iovane G., Marino A. et al., 2002, *A&A*, 381, 845.
- Calchi Novati S., Jetzer Ph., Scarpetta G. et al., 2003, *A&A*, 405, 851.
- Calchi Novati S., Paulin-Henriksson S., Baillon P., et al., 2005, astro-ph 0504188, to appear in *A&A*.
- Crofts A. P. S., 1992, *ApJ*, 399, L43.
- de Jong J. T. A., Kuijken K., Crofts A. P. S. et al., 2004, *A&A*, 417, 461.
- De Paolis F., Ingrosso G., Nucita A. & Zakharov A. F., 2005, *A&A*, 432, 501.
- De Rújula A., Jetzer Ph. & Masso E., 1991, *MNRAS* 250, 348.
- Gondolo P., 1999, *ApJ*, 510, L29.
- Gould A., Bahcall J.N. & Flynn C., 1997, *ApJ*, 482, 913.
- Griest K., 1991, *ApJ*, 366, 412.
- Gyuk G. & Crofts A. P. S., 2000, *ApJ*, 535, 621.
- Jetzer Ph., 1994, *A&A*, 286, 426.
- Jetzer, Ph., Milsztajn, A. & Tisserand, P., 2004, in the proceedings of the IAU Symposium No. 225 eds. Y. Mellier & G. Meylan (Cambridge University Press 2005) p. 339.
- Jetzer Ph., Mancini L. & Scarpetta G., 2002, *A&A*, 393, 129.
- Joshi, Y.C., Pandey, A.K., Narasimha, D., & Sagar, R. 2005, *A&A* 433, 787 .
- Kent S. M., 1989, *AJ*, 97, 1614.
- Kerins E., Carr B., Ewans N.W. et al., 2001, *MNRAS*, 323, 13.
- Kerins E., An J., Ewans N. W. et al., 2003, *ApJ*, 598, 993.
- Kerins E., 2004, *MNRAS*, 347, 1033.
- Kerins E., Darnley M.J., Duke J. et al., 2005, astro-ph 0502545.
- Mamon G. A. & Soneira R. M., 1982, *ApJ*, 255, 181.
- Navarro J.F., Frenk C.S. & White S.D.M., 1997, *ApJ*, 490, 493.
- Paczynski B., 1986, *ApJ*, 304, 1.
- Paulin-Henriksson S., Baillon P., Bouquet A. et al., 2003, *A&A*, 405, 15.
- Riffeser A., Fliri J., Bender R. et al., 2003, *ApJ*, 599, L17.
- Stark A. & Binney J., 1994, *ApJ*, 426, L31.
- Uglesich R. R., Crofts A. P. S., Baltz E. A., et al. 2004, *ApJ*, 588, 311